

PROCEEDINGS OF SPIE

Photonics Applications in Astronomy, Communications, Industry, and High Energy Physics Experiments 2020

Ryszard S. Romaniuk
Maciej Linczuk
Editors

31 August – 6 September 2020
Wilga, Poland

Organized by
Institute of Electronic Systems, Faculty of Electronics and Information Technologies, Warsaw
University of Technology (Poland)

Sponsored by
PSP—Photonics Society of Poland • Committee of Electronics and Telecommunications of Polish
Academy of Sciences • ARIES—Accelerator Research and Innovation for European Science and
Society (CERN, EU H2020) • PKOpto—Polish Committee of Optoelectronics of SEP, The Association
of Polish Electrical Engineers • EuroFusion Poland

Published by
SPIE

Volume 11581

Proceedings of SPIE 0277-786X, V. 11581

SPIE is an international society advancing an interdisciplinary approach to the science and application of light.

Photonics Applications in Astronomy, Communications, Industry, and High Energy Physics Experiments 2020
edited by Ryszard S. Romaniuk, Maciej Linczuk, Proc. of SPIE Vol. W1200, W120000
© 2020 SPIE · CCC code: 0277-786X/20/\$21 · doi: 10.1117/12.2585818

Proc. of SPIE Vol. W1200 1158101-1

The papers in this volume were part of the technical conference cited on the cover and title page. Papers were selected and subject to review by the editors and conference program committee. Some conference presentations may not be available for publication. Additional papers and presentation recordings may be available online in the SPIE Digital Library at SPIEDigitalLibrary.org.

The papers reflect the work and thoughts of the authors and are published herein as submitted. The publisher is not responsible for the validity of the information or for any outcomes resulting from reliance thereon.

Please use the following format to cite material from these proceedings:

Author(s), "Title of Paper," in *Photonics Applications in Astronomy, Communications, Industry, and High Energy Physics Experiments 2020*, edited by Ryszard S. Romaniuk, Maciej Linczuk, Proceedings of SPIE Vol. 11581 (SPIE, Bellingham, WA, 2020) Seven-digit Article CID Number.

ISSN: 0277-786X
ISSN: 1996-756X (electronic)

ISBN: 9781510639874
ISBN: 9781510639881 (electronic)

Published by

SPIE

P.O. Box 10, Bellingham, Washington 98227-0010 USA
Telephone +1 360 676 3290 (Pacific Time) · Fax +1 360 647 1445

SPIE.org

Copyright © 2020, Society of Photo-Optical Instrumentation Engineers.

Copying of material in this book for internal or personal use, or for the internal or personal use of specific clients, beyond the fair use provisions granted by the U.S. Copyright Law is authorized by SPIE subject to payment of copying fees. The Transactional Reporting Service base fee for this volume is \$21.00 per article (or portion thereof), which should be paid directly to the Copyright Clearance Center (CCC), 222 Rosewood Drive, Danvers, MA 01923. Payment may also be made electronically through CCC Online at copyright.com. Other copying for republication, resale, advertising or promotion, or any form of systematic or multiple reproduction of any material in this book is prohibited except with permission in writing from the publisher. The CCC fee code is 0277-786X/20/\$21.00.

Printed in the United States of America by Curran Associates, Inc., under license from SPIE.

Publication of record for individual papers is online in the SPIE Digital Library.

**SPIE. DIGITAL
LIBRARY**

SPIEDigitalLibrary.org

Paper Numbering: *Proceedings of SPIE* follow an e-First publication model. A unique citation identifier (CID) number is assigned to each article at the time of publication. Utilization of CIDs allows articles to be fully citable as soon as they are published online, and connects the same identifier to all online and print versions of the publication. SPIE uses a seven-digit CID article numbering system structured as follows:

- The first five digits correspond to the SPIE volume number.
- The last two digits indicate publication order within the volume using a Base 36 numbering system employing both numerals and letters. These two-number sets start with 00, 01, 02, 03, 04, 05, 06, 07, 08, 09, 0A, 0B ... 0Z, followed by 10-1Z, 20-2Z, etc. The CID Number appears on each page of the manuscript.

Contents

PHOTONICS APPLICATIONS IN ASTRONOMY, COMMUNICATIONS, INDUSTRY, AND HIGH-ENERGY PHYSICS EXPERIMENTS 2020

- 11581 02 **Photonics Applications and Web Engineering: WILGA 2020** [11581-1]
- 11581 03 **Using the conformable fractional derivative in Caputo sense operator to describe the behavior of an RC electrical circuit containing a supercapacitor** [11581-2]
- 11581 04 **Adaptation of the therminator model for BES program (Invited Paper)** [11581-3]
- 11581 05 **Teaching electronics in time of disease: virtual laboratory for Linux in embedded systems** [11581-4]
- 11581 06 **Pion-kaon femtoscopy in Therminator 2 model** [11581-5]
- 11581 07 **Femtoscopy of particles with strange quark** [11581-6]
- 11581 08 **Multimodal emotion classification by streaming fixed time segments for speaker movies (Invited Paper)** [11581-7]
- 11581 09 **Current trends in ship detection in single polarization synthetic aperture radar imagery** [11581-8]
- 11581 0A **Open system for measuring the chemiluminescence of crop seeds** [11581-9]
- 11581 0B **Fluorescent microscopy of biological tissues of the dead with the different levels of blood loss** [11581-10]
- 11581 0C **NIR spectroscopy for automated grain analyzers** [11581-11]
- 11581 0D **Polarization-phase diagnostics of volume of blood loss** [11581-12]
- 11581 0E **A function-based approach to real-time visualization using graphics processing units** [11581-13]
- 11581 0F **Q-processors for real-time image processing** [11581-14]
- 11581 0G **MESH concept for mobile distribution point architecture of ICT infrastructure (Invited Paper)** [11581-15]
- 11581 0H **Concept of the simulation platform architecture for the operational data aggregation platform** [11581-16]

PROCEEDINGS OF SPIE

[SPIDigitalLibrary.org/conference-proceedings-of-spie](https://spiedigitallibrary.org/conference-proceedings-of-spie)

Fluorescent microscopy of biological tissues of the dead with the different levels of blood loss

Ushenko, Olexander, Syvokorovskaya, Anna, Bachinsky, Victor, Garazdyuk, Marta, Vanchuliak, Oleg, et al.

Olexander Ushenko, Anna Syvokorovskaya, Victor Bachinsky, Marta Garazdyuk, Oleg Vanchuliak, Olexander Dubolazov, Yuriy Ushenko, Yuriy Tomka, Mykhaylo Gorsky, Iryna Soltys, Zbigniew Omiotek, Nataliia Kondratiuk, Aigul Iskakova, "Fluorescent microscopy of biological tissues of the dead with the different levels of blood loss," Proc. SPIE 11581, Photonics Applications in Astronomy, Communications, Industry, and High Energy Physics Experiments 2020, 115810B (14 October 2020); doi: 10.1117/12.2580194

SPIE.

Event: Photonics Applications in Astronomy, Communications, Industry, and High Energy Physics Experiments 2020, 2020, Wilga, Poland

Fluorescent microscopy of biological tissues of the dead with the different levels of blood loss

Olexander Ushenko^{*a}, Anna Syvokorovskaya^b, Victor Bachinsky^b, Marta Garazdyuk^b,
Oleg Vanchuliak^b, Olexander Dubolazov^a, Yuriy Ushenko^a, Yuriy Tomka^a, Mykhaylo Gorsky^a,
Iryna Soltys^a, Zbigniew Omiotek^c, Nataliia Kondratiuk^d, Aigul Iskakova^e
^aChernivtsi National University, 2 Kotsiubynskyi Str., Chernivtsi, Ukraine, 58012; ^bBukovinian
State Medical University, 3 Theatral Sq., Chernivtsi, Ukraine, 58000; ^cLublin University of
Technology, ul. Nadbystrzycka 38d, 20-618 Lublin, Poland; ^dOles Honchar Dnipro National
University, Haharina Ave, 72, 49000 Dnipro, Ukraine; ^eSatbayev Kazakh National Technical
University, Almaty, Kazakhstan

ABSTRACT

The results of laser autofluorescence microscopy of the distribution of the intensity of the multidimensional laser autofluorescence (MLA) microscopy of polycrystalline structures of biological tissue preparations are presented. The data of a statistical analysis of the distribution of the magnitude of the intensity of MLA networks of biological crystals of histological sections of tissues of the spleen with the parenchymal morphological structure of the dead are presented.

Keywords: Autofluorescent microscopy, degree of blood loss, biological tissue, correlation, diagnostics.

1. INTRODUCTION

The Figure 1 presents a functional block diagram of spectrally selective laser autofluorescence microscopy of parenchymal biological tissues^{1,2,3}.

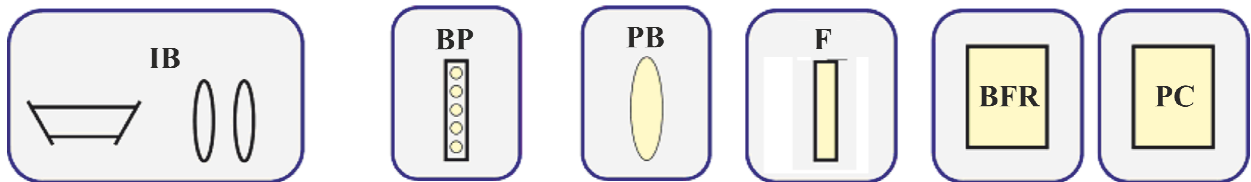


Figure 1. Functional block diagram of multidimensional spectrally selective laser autofluorescence microscopy.

The illumination block **IB** consisting of a laser and a collimator ensures the formation of a polarized parallel laser beam of 2mm in diameter and wavelength of 405nm, which excites the intrinsic fluorescence of the fluorophores of biological preparations^{4,5,6}. The object block **OB** is a microscopic table with a two-coordinate movement on which the biological preparation **BP** is attached. The projection block **PB**, which with the help of the micro-lens **MO** (4X) ensures the formation of a self-fluorescence microscopic image of a biological preparation **BP** excited by a laser beam in the plane of the digital camera **DC**. The block of spectral filtration of BF, which includes the interference light filters **F** for the spectral selection of the excited self-fluorescence polychromatic radiation of an ensemble of **BP** fluorophores. Block of photoelectron registration **BFR** of microscopic fluorescent images of biological preparations **BP**, provides the formation of the coordinate digital distribution of the intensity value in the computer interface. The data processing block **DPB** using a personal computer **PC** provides a calculation of the magnitude of the statistical moments of the 1st to 4th orders characterizing the intensity distribution of the spectrally selective autofluorescence of biological preparations **BP**.

2. SAMPLES

2.1 The spleen

Depending on the level of blood loss, the following groups of samples of histological sections of the spleen with the subsequent level of blood loss were considered: $V=0\text{mm}^3$ – group 1 (samples); $V=500\text{mm}^3\pm 100\text{mm}^3$ – group 2 (samples); $V=1000\text{mm}^3\pm 100\text{mm}^3$ – group 3 (samples); $V=1500\text{mm}^3\pm 100\text{mm}^3$ – group 4 (samples); $V=2000\text{mm}^3\pm 100\text{mm}^3$ – group 5 (samples); $V=2500\text{mm}^3\pm 100\text{mm}^3$ – group 6 (samples).

On a series of fragments of fig. 2 shows the experimentally determined coordinate distributions (fragments (1), (3)) and histograms (fragments (2), (4)) random values of the fluorescence intensity of the parenchymal structure of histological sections of the spleen of the dead from group 1 (fragments (1), (2)) and groups 3 (fragments (3), (4)).

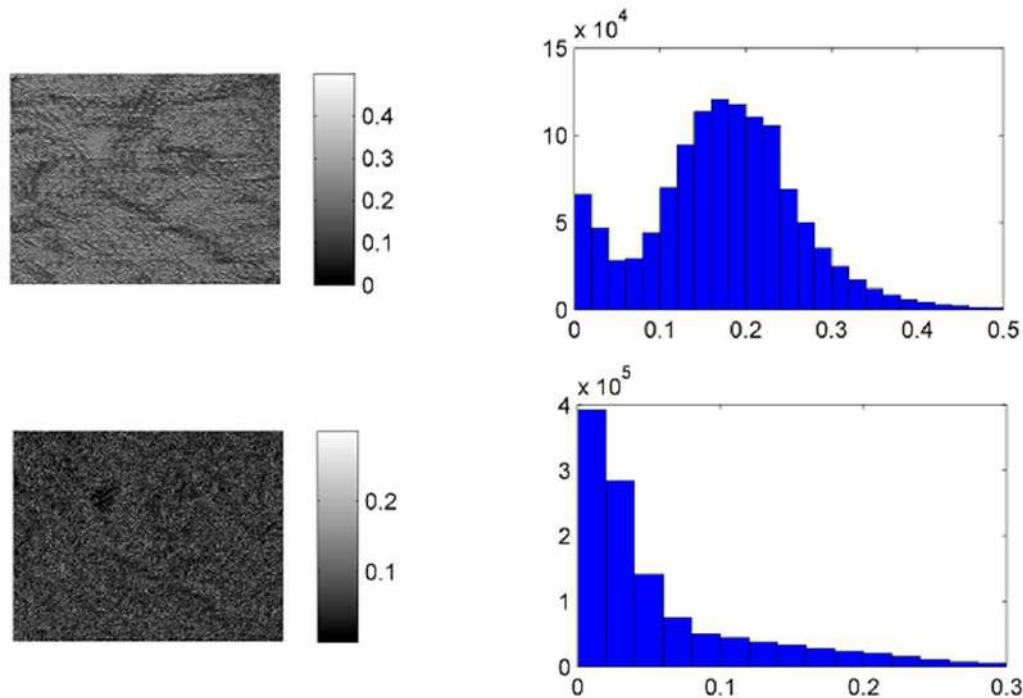


Figure 2. Maps ((1), (3)) and histograms ((2), (4)) distributions of the autofluorescence intensity values of histological sections of the spleen of the control ((1), (2)) and research ((3), (4)) groups the dead.

Quantitatively, the scenario of changes in the fluorescent properties of an ensemble of blood cells of the parenchymal structure of the histological sections of the spleen of the dead with varying degrees of blood loss is illustrated by the statistical moments of the 1st – 4th orders given in Table 1^{7,8,9}.

The following values were established:

- the range of changes in the magnitude of the 1st to 4th order statistical momentum, which characterizes the distribution of the intensity of MLA in the parenchymal structures of the histological sections of the spleen, by volume of blood loss is $0 \text{ mm}^3 \div 2500 \text{ mm}^3$;
- the average magnitude SM_1 varies within the range of averages from 0.17 to 0.04;
- the dispersion magnitude SM_2 varies the range of averages from 0.09 to 0.025;
- the asymmetry magnitude SM_3 varies the range of averages from 0.25 to 2.31;
- the kurtosis magnitude SM_4 varies the range of averages from 0.72 to 2.88.

Fig. 3 shows diagrams of changes in the magnitude of the statistical moments characterizing the distribution of the magnitude of the laser autofluorescence intensity of histological sections of the spleen as a result of the blood loss of all groups of the deceased^{10,11,12}.

Table 1. The statistical structure of the autofluorescence intensity maps of histological sections of the spleen of the dead with varying degrees of blood loss.

Blood loss, mm³	0	500 ± 100 mm³	1000 ± 100 mm³
The average , SM_1	0.17 ± 0.007	0.14 ± 0.006	0.11 ± 0.0045
Criteria, t, p	$p < 0.05$	$p < 0.05$	$p < 0.05$
The average , SM_2	0.09 ± 0.004	0.07 ± 0.003	0.055 ± 0.002
Criteria, t, p	$p < 0.05$	$p < 0.05$	$p < 0.05$
The average , SM_3	0.25 ± 0.011	0.75 ± 0.034	1.22 ± 0.058
Criteria, t, p	$p < 0.05$	$p < 0.05$	$p < 0.05$
The average , SM_4	0.72 ± 0.029	1.11 ± 0.051	1.53 ± 0.069
Criteria, t, p	$p < 0.05$	$p < 0.05$	$p < 0.05$
Blood loss, mm³	1500 ± 100 mm³	2000 ± 100 mm³	2500 ± 100 mm³
The average , SM_1	0.09 ± 0.004	0.07 ± 0.003	0.04 ± 0.002
Criteria, t, p	$p < 0.05$	$p < 0.05$	$p < 0.05$
The average , SM_2	0.045 ± 0.002	0.032 ± 0.001	0.025 ± 0.001
Criteria, t, p	$p < 0.05$	$p < 0.05$	$p < 0.05$
The average, SM_3	1.77 ± 0.075	2.02 ± 0.096	2.31 ± 0.11
Criteria, t, p	$p < 0.05$	$p < 0.05$	$p < 0.05$
The average, SM_4	1.96 ± 0.098	2.34 ± 0.11	2.88 ± 0.13
Criteria, t, p	$p < 0.05$	$p < 0.05$	$p < 0.05$

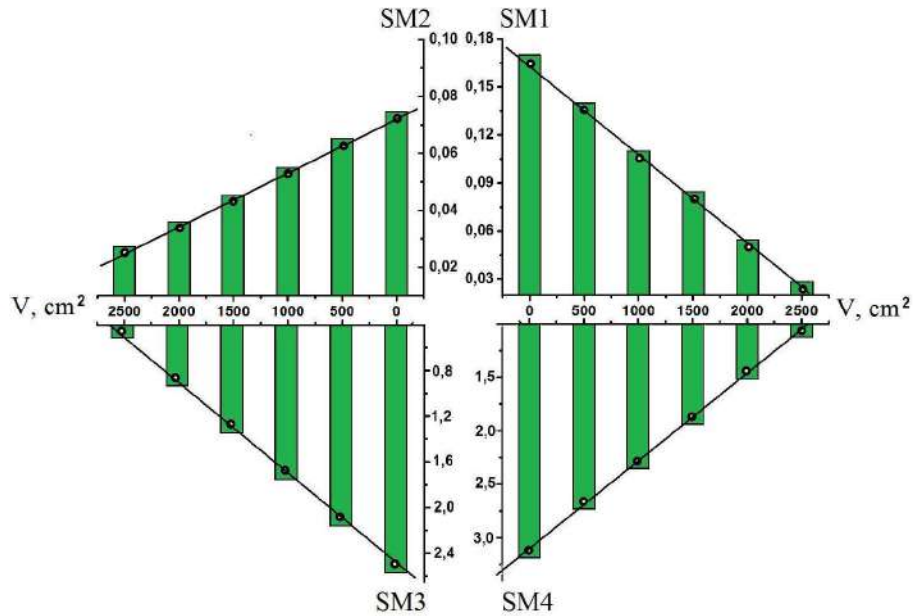


Figure 3. Dependencies of the magnitude of the average (1), dispersion (2), asymmetry (3) and excess (4), which characterize the autofluorescence intensity maps of histological sections of the spleen of the deceased with varying degrees of blood loss.

The results of the method of spectral-selective laser autofluorescence microscopy (Fig. 3) show that the dynamics of changes in the magnitude of the statistical moments (average (1), dispersion (2), asymmetry (3) and excess (4)) characterizing the distribution of the fluorescence blood elements histological sections of the spleen of the dead, vary within the volume of blood loss $0 \text{ mm}^3 \div 2500 \text{ mm}^3$. The most sensitive to MLA parenchymatous structures of histological sections of this organ to statistical parameters of the 2nd to 4th orders were established^{13,14,15}.

2.2 Kidney

Maps (fragments (1), (3)) and histograms (fragments (2), (4)) of MLA intensity distributions of polycrystalline structures of samples of histological sections of the kidney of the deceased from group 1 (fragments (1), (2)) and group 3 (fragments (3), (4)), which were obtained by the method of spectral-selective laser autofluorescence microscopy, are shown in a series of dependences of Figs. 4.

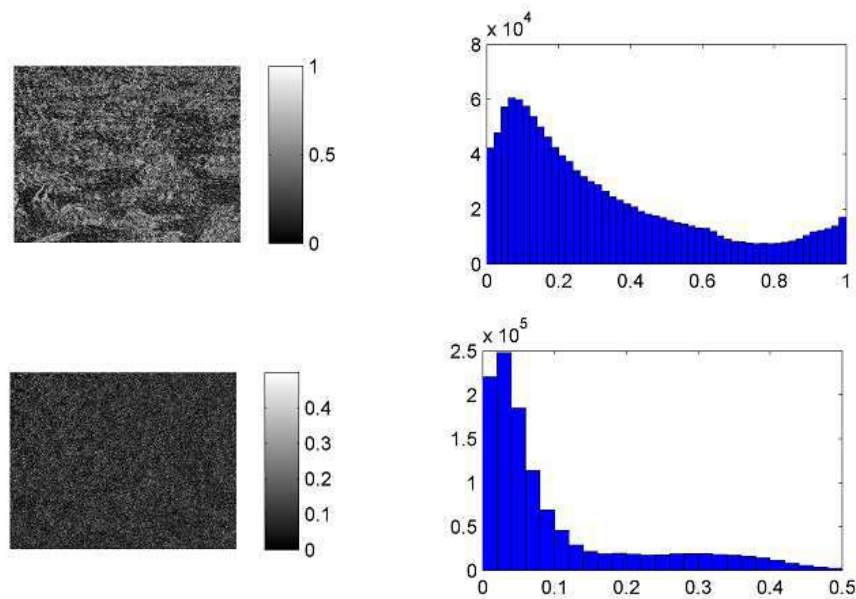


Figure 4. Maps ((1), (3)) and histograms (histories (2), (4)) of distributions of the value of autofluorescence intensity of histological sections of the kidney of the control ((1), (2)) and experimental ((3), (4)) groups of the dead.

Analysis of the obtained data revealed that with increasing blood loss and a corresponding decrease in the concentration of formed blood elements decreases the fluorescence intensity of optically anisotropic collagen networks of the kidneys of the deceased (Fig. 4, fragments (2), (4)).

Such changes are manifested in a decrease in the values of the corresponding statistical parameters - mean and variance, which characterize the distributions of the MLA intensity of histological sections of kidney tissue of all groups of the dead. In parallel, the values of the statistical moments of the 3rd and 4th orders increase, which characterize the asymmetry and excess of the distributions of the corresponding MLA histological sections of the kidneys of the dead in the range of blood loss to $V=2500\text{mm}^3 \pm 100\text{mm}^3$.

Data from statistical analysis of changes in the structure of MLA samples of histological sections of the kidneys of the deceased with varying degrees of blood loss illustrate the statistical moments of the 1st - 4th orders, the values of which are given in table 2^{16,17,18}.

The following values were established:

- the statistical moment of the 1st order changes within the range of change of average values from 0,32 to 0,04;
- the statistical moment of the 2nd order changes within the range of change of average values from 0,26 to 0,03;
- the statistical moment of the 3rd order changes within the range of change of average values from 0,97 to 2,51;
- the statistical moment of the 4th order changes within the range of change of average values from 0,51 to 2,89.

Table 2. Statistical structure of autofluorescence intensity maps of histological sections of the kidneys of the dead with different degrees of blood loss

Blood loss, mm ³	0	500 ± 100 mm ³	1000 ± 100 mm ³
The average, SM_1	0.32 ± 0.013	0.26 ± 0.012	0.21 ± 0.011
Criteria, t, p	$p < 0.05$	$p < 0.05$	$p < 0.05$
Dispersion, SM_2	0.26 ± 0.012	0.21 ± 0.011	0.16 ± 0.07
Criteria, t, p	$p < 0.05$	$p < 0.05$	$p < 0.05$
Asymmetry, SM_3	0.97 ± 0.045	1.33 ± 0.062	1.61 ± 0.074
Criteria, t, p	$p < 0.05$	$p < 0.05$	$p < 0.05$
Kurtosis, SM_4	0.51 ± 0.022	1.04 ± 0.043	1.69 ± 0.078
Criteria, t, p	$p < 0.05$	$p < 0.05$	$p < 0.05$
Blood loss, mm ³	1500 ± 100 mm ³	2000 ± 100 mm ³	2500 ± 100 mm ³
The average, SM_1	0.16 ± 0.007	0.09 ± 0.004	0.04 ± 0.002
Criteria, t, p	$p < 0.05$	$p < 0.05$	$p < 0.05$
Dispersion, SM_2	0.11 ± 0.005	0.07 ± 0.003	0.03 ± 0.001
Criteria, t, p	$p < 0.05$	$p < 0.05$	$p < 0.05$
Asymmetry, SM_3	1.92 ± 0.089	2.23 ± 0.11	2.51 ± 0.12
Criteria, t, p	$p < 0.05$	$p < 0.05$	$p < 0.05$
Kurtosis, SM_4	2.02 ± 0.096	2.43 ± 0.11	2.89 ± 0.13
Criteria, t, p	$p < 0.05$	$p < 0.05$	$p < 0.05$

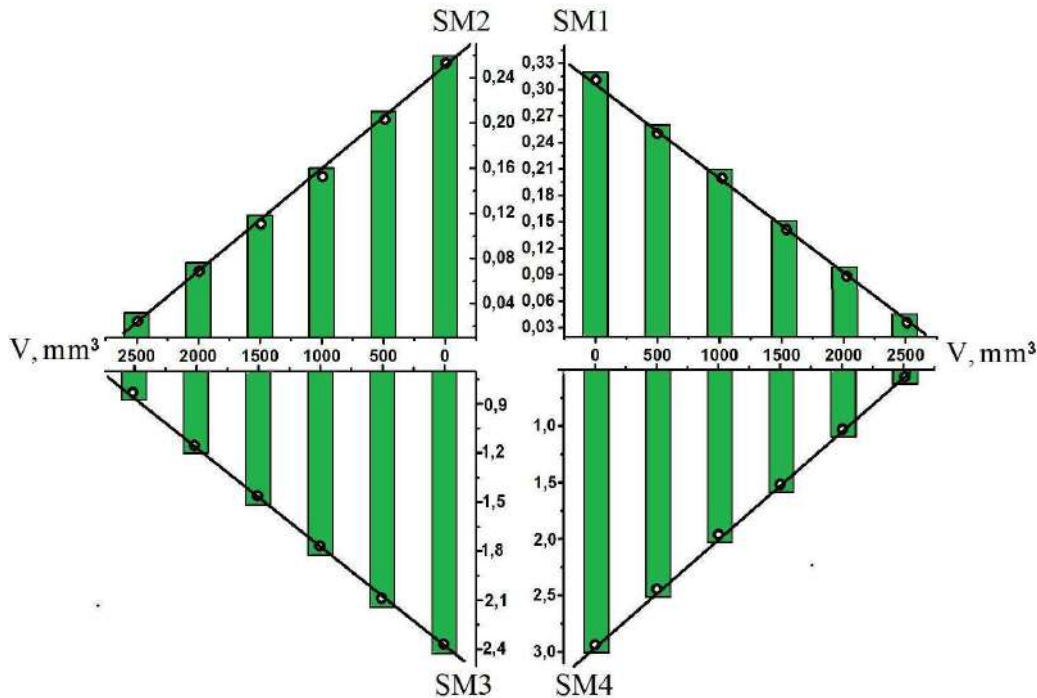


Figure 5. Dependencies of the magnitude of the average (1), dispersion (2), asymmetry (3) and excess (4), which characterize the autofluorescence intensity maps of histological sections of the kidney of the deceased with varying degrees of blood loss.

Figure 5 presents diagrams of changes in the set of statistical moments of the 1st – 4th orders, which characterize the coordinate structure of the distributions of random values of laser autofluorescence (MLA) optically anisotropic collagen networks of the set of histological sections of the kidneys of the dead from all groups^{18,19}

Statistical analysis of laser spectral-selective laser autofluorescence microscopy of optically anisotropic grids of biological crystals revealed (Fig. 4, Table 2) a decrease in the mean, dispersion and, conversely, an increase in asymmetry and excess, which characterize the intensity distributions of MLA within the volume of blood loss. The statistical moments of the 1st, 2nd and 4th orders were the most sensitive to changes in the fluorescence intensity of ensembles of formed blood elements of histological sections of the kidney with different levels of blood loss $V=2500\text{mm}^3\pm 100\text{mm}^3$.

3. THE EFFECTIVENESS OF THE DIFFERENTIAL DIAGNOSIS OF THE DEGREE OF BLOOD LOSS BY LASER AUTOFLUORESCENCE MICROSCOPY

For each statistical moment that characterizes the distribution of the MLA intensity values of a set of spleen samples from different groups of deceased, the accuracy of determining the blood loss volume was found on the basis of a series of nomograms presented in Fig. 4.

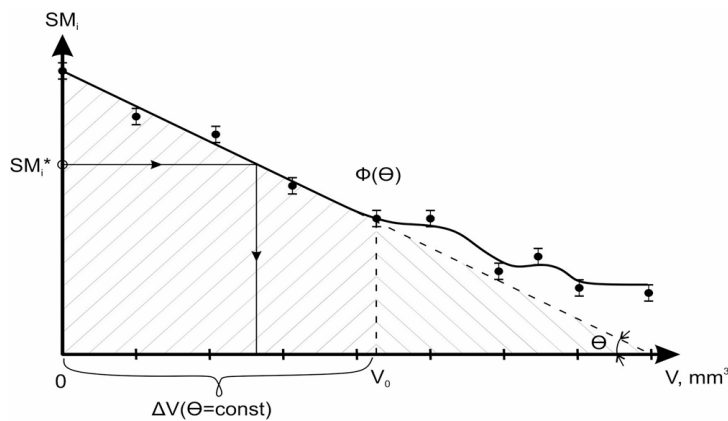


Figure 6. Analytical scheme for determining the volume of blood loss according to the method of laser autofluorescence microscopy.

Table 3. Accuracy of determining the volume of blood loss in the spleen

Blood loss, mm^3	$500\pm 100 \text{ mm}^3$	$1000\pm 100\text{mm}^3$	$1500\pm 100\text{mm}^3$	$2000\pm 100\text{mm}^3$	$2500\pm 100\text{mm}^3$
Average, SM_1	84	86	86	84	84
Dispersion, SM_2	94	94	92	92	90
Asymmetry, SM_3	96	94	94	92	90
Kurtosis, SM_4	92	92	92	90	88

Table 4. Accuracy in determining the amount of blood loss in the kidney

Blood loss, mm^3	$500\pm 100 \text{ mm}^3$	$1000\pm 100\text{mm}^3$	$1500\pm 100\text{mm}^3$	$2000\pm 100\text{mm}^3$	$2500\pm 100\text{mm}^3$
Average, SM_1	96	96	96	94	94
Dispersion, SM_2	96	96	94	92	92
Asymmetry, SM_3	84	86	86	86	84
Kurtosis, SM_4	94	94	92	90	90

The analysis of the obtained data revealed the following parameters of the diagnostic efficiency of the statistical analysis of the results of the method of spectrally selective laser autofluorescence microscopy of histological sections of parenchymal biological tissues:

1. For all studied biological preparations, the range of sensitivity of the method of spectral-selective laser autofluorescence microscopy to changes in the volume of blood loss of the dead is the maximum level $0 \text{ mm}^3 \div 2500 \text{ mm}^3$.
2. The accuracy of the method of spectral-selective laser autofluorescence microscopy of biological samples varies in the range: $\Delta V = 0 \text{ mm}^3 \div 2500 \text{ mm}^3 \leftrightarrow 86\% \div 92\%$
3. The maximum level is reached for the following statistical parameters characterizing laser autofluorescence maps of histological sections of the spleen –

$$\begin{cases} SM_1 \leftrightarrow 90\% - 94\%; \\ SM_2 \leftrightarrow 92\% - 96\%; \\ SM_3 \leftrightarrow 88\% - 92\%; \end{cases}$$

CONCLUSION

The research resulted in the following conclusions:

1. A set of maps and histograms of random fluorescence intensity distributions of blood corpuscles of the polycrystalline component of histological sections of parenchymal biological tissues of the spleen of the deceased with varying degrees of blood loss were studied using spectral-selective laser autofluorescence microscopy.
2. The dynamics of changes in the magnitude of the statistical moments of the 1st – 4th orders, characterizing the distribution of MLA histological sections of parenchymal (spleen) tissues of the deceased with different blood loss - $\Delta V = 0 \text{ mm}^3 \div 2500 \text{ mm}^3$, was studied.
3. The magnitudes and ranges of the accuracy of the method of spectral-selective laser autofluorescent microscopy of biological preparations of the spleen are determined as $SM_2 \leftrightarrow 90\% \div 94\%$ and $SM_3 \leftrightarrow 92\% \div 96\%$ and $SM_4 \leftrightarrow 88\% \div 92\%$.

REFERENCES

- [1] M. K. Swami, H. S. Patel, and P. K. Gupta, "Conversion of 3×3 Mueller matrix to 4×4 Mueller matrix for non-depolarizing samples," *Opt. Commun.* 286(1), 18–22 (2013).
- [2] V. F. Izotova et al., "Investigation of Mueller matrices of anisotropic nonhomogeneous layers in application to optical model of cornea," *Appl. Opt.* 36(1), 164–169 (1997).
- [3] V. V. Tuchin, "Tissue optics and photonics: biological tissue structures [review]," *J. Biomed. Photonics Eng.* 1(1), 3–21 (2015).
- [4] V. V. Tuchin, "Tissue optics and photonics: light-tissue interaction [review]," *J. Biomed. Photonics Eng.* 1(2), 98–134 (2015).
- [5] S. Bartel and A. H. Hielscher, "Monte Carlo simulations of the diffuse backscattering Mueller matrix for highly scattering media," *Appl. Opt.* 39, 1580–1588 (2000).
- [6] Kozlovskaya, T. I., Kolisnik, P. F., Zlepko, S. M., et al., "Physical-mathematical model of optical radiation interaction with biological tissues," *Proc. SPIE* 10445, (2017).
- [7] X. Wang and L. V. Wang, "Propagation of polarized light in birefringent turbid media: a Monte Carlo study," *J. Biomed. Opt.* 7(3), 279–290 (2002).
- [8] M.-R. Antonelli et al., "Impact of model parameters on Monte Carlo simulations of backscattering Mueller matrix images of colon tissue," *Biomed. Opt. Express* 2(7), 1836–1851 (2011).
- [9] M. R. Antonelli et al., "Mueller matrix imaging of human colon tissue for cancer diagnostics: how Monte Carlo modeling can help in the interpretation of experimental data," *Opt. Express* 18(10), 10200–10208 (2010).
- [10] I. A. Vitkin and R. C. N. Studinski, "Polarization preservation in diffusive scattering from in vivo turbid biological media: effects of tissue optical absorption in the exact backscattering direction," *Opt. Commun.* 190, 37–43 (2001).

- [11] Y. P. Sinichkin et al., "Reflectance and fluorescence spectroscopy of human skin in vivo," in Handbook of Optical Biomedical Diagnostics, 2nd ed., V. V. Tuchin, Ed., pp. 95–185, SPIE Press, Bellingham, Washington (2016).
- [12] Ushenko, V.A., Sidor, M.I., Marchuk, Yu.F., Pashkovskaya, N.V., Andreichuk, D.R. Azimuth-invariant mueller-matrix differentiation of the optical anisotropy of biological tissues (2014) Optics and Spectroscopy (English translation of Optika i Spektroskopiya), 117 (1), pp. 152-157.
- [13] Ushenko, V.A., Pavlyukovich, N.D., Trifonyuk, L. Spatial-frequency azimuthally stable cartography of biological polycrystalline networks (2013) International Journal of Optics, 2013, 683174 .
- [14] Ushenko, V.A., Zabolotna, N.I., Pavlov, S.V., Burcovets, D.M., Novakovska, O.Yu. Mueller-matrices polarization selection of two-dimensional linear and circular birefringence images (2013) Proceedings of SPIE - The International Society for Optical Engineering, 9066, 90661X .
- [15] Methods of Processing Video Polarimetry Information Based on Least-Squares and Fourier Analysis // RH Rovira, SV Pavlov, OS Kaminski, MM Bayas - Middle-East Journal of Scientific Research, T. 16 (9), 1201-1204 2013. – P.1201-1204.
- [16] N. I. Zabolotna; S. V. Pavlov; A. G. Ushenko; A. O. Karachevtsev; V. O. Savich, et al. System of the phase tomography of optically anisotropic polycrystalline films of biological fluids, Proc. SPIE 9166, Biosensing and Nanomedicine VII, 916616 (August 27, 2014)
- [17] N. I. Zabolotna; S. V. Pavlov; A. G. Ushenko; O. V. Sobko and V. O. Savich. Multivariate system of polarization tomography of biological crystals birefringence networks, Proc. SPIE 9166, Biosensing and Nanomedicine VII, 916615 (August 27, 2014); doi:10.1117/12.2061105.
- [18] Dzierżak, R., "Comparison of the influence of standardization and normalization of data on the effectiveness of spongy tissue texture classification," Informatyka, Automatyka, Pomiary w Gospodarce i Ochronie Środowiska 9(3), 66-69 (2019). <https://doi.org/10.35784/iapgos.62>
- [19] S. Y. Tuzhanskyy, "Methods and means of polarization parameter control in biotissue imaging polarimetry", Proc. SPIE 6682, Polarization Science and Remote Sensing III, 668212 (26 October 2007).